

Pro-arrhythmogenic effects of heterogeneous tissue curvature: Role of left atrial appendage in atrial fibrillation

*Jun-Seop Song, Young-Seon Lee, Byoung-hyun Lim, Minki Hwang, Boyoung Joung, Hui-Nam Pak**

Yonsei University College of Medicine, Seoul, Republic of Korea

Running title: Arrhythmogenic role of bumpy LAA

Abstract

Aims The arrhythmogenic role of atrial complex morphology such as left atrial appendage (LAA) has not yet been clearly elucidated. We hypothesized that bumpy tissue geometry can induce action potential duration (APD) dispersion and wavebreak in atrial fibrillation (AF).

Methods We simulated 2D-bumpy atrial model by varying the degree of bumpiness and 3D-left atrial (LA) model of 14 patients with persistent AF. Additionally, in 30 patients with persistent AF, we analyzed curvature map of LA geometry, and complex fractionated atrial electrogram-cycle length (CFAE-CL), Shannon entropy (ShEn), and approximate entropy (ApEn) of bipolar electrogram.

Results In 2D-bumpy model, APD dispersion increased with increasing surface bumpiness ($p<0.001$), and wavebreak occurred spontaneously when the surface bumpiness was higher, showing phase transition-like behavior ($p<0.001$). Additionally, 2D-bumpy model with bumpiness gradient showed that spiral wave drifted in the direction of higher bumpiness, and phase singularity (PS) points were mostly located in areas with higher bumpiness. In 3D-LA model, PS density was higher in LAA compared to other LA parts ($p<0.05$). In 30 persistent AF patients, the surface bumpiness of LAA was 5.8-times that of other LA parts ($p<0.001$), and exceeded critical bumpiness to induce wavebreak. Also, all clinical wave dynamics parameters of bipolar electrogram were significantly dominant in LAA ($p<0.001$).

Conclusion The bumpy tissue geometry promotes APD dispersion, wavebreak, and spiral wave drift in *in-silico* human atrial tissue. Both simulation results and dominant clinical wave dynamics parameters in LAA imply that LAA is an arrhythmogenic bumpy structure in AF.

Key Words: *Atrial fibrillation, Modeling, Curvature, Action potential duration, Spiral wave dynamics, Left atrial appendage*

Competing interests: The authors declare no competing financial interests.

1. Introduction

Atrial fibrillation (AF) is one of the most common cardiac arrhythmias that increases the risk of cardioembolic stroke and mortality. Although pulmonary vein isolation (PVI) is an effective treatment for AF, PVI-only ablation is not sufficient particularly in patients with persistent AF¹. In 2010, Di Biase et al. reported that the left atrial appendage (LAA) was found to be responsible for atrial arrhythmias in 27% of patients undergoing redo ablation². Several other clinical studies support that the LAA is a potential extrapulmonary source of atrial arrhythmias and LAA isolation is effective for the treatment of persistent AF³⁻⁶. However, how the LAA play a pro-arrhythmic role in the maintenance of AF has not been clearly revealed.

One of the significant features of the LAA is its complex bumpy morphology^{7,8}. Several computational and experimental studies have shown that the uneven tissue geometry induce dispersion of action potential duration (APD)^{9,10} and change spiral wave dynamics^{8,11,12}. Rogers¹³ reported that nonzero Gaussian curvature (briefly, ‘curvature’) of tissue geometry altered wave propagation speed and APD, and abrupt change of curvature could promote wavebreak in ventricular geometry. Despite being studied previously, the mechanism of change of spiral wave dynamics in the bumpy atrial tissue and its arrhythmogenic role in human AF have not been clearly established.

We hypothesized that bumpy tissue geometry could play a pro-arrhythmic role in AF. We studied the effects of heterogeneous curvature on spatial dispersion of APD and wavebreak in *in-silico* human atrial tissue by varying the degree of bumpiness. To determine the pro-arrhythmic effects of bumpy feature in real LA geometry, we simulated 3D-left atrial (LA) model reflecting the LA geometry of AF patients. Additionally, we measured surface bumpiness of the LAA, and estimated wave dynamics parameters from clinically obtained bipolar electrogram, such as complex fractionated atrial electrogram (CFAE) and entropy parameters (Shannon and approximate entropy), which are known to be related to wavebreak¹⁴ and rotational activation^{15,16}.

2. Methods

2.1. Computational model of bumpy surface

We simulated homogeneous, isotropic bumpy tissue consisting of 512×512 human atrial cells ($\Delta x=0.025$ cm). We designed periodically bumpy patterns by varying the degree of bumpiness as the following equation:

$$z = A \sin\left(\frac{2\pi kx}{L}\right) \cos\left(\frac{2\pi ky}{L}\right)$$

where L is the size of the tissue, x, y are coordinates of the cells, A is the amplitude of curves, and k is the number of periodic curves. We constructed 24 surfaces by varying the amplitude of curves A=1~6 mm and the number of periodic curves k=1~4 (Fig. S1). We considered the flat tissue as the control case.

A biophysical model of the human atrial myocyte¹⁷ was implemented. No electrical remodeling was assumed to determine the pure effect of bumpy geometry on wavebreak. We calculated electrical conduction by the following reaction-diffusion equation:

$$\frac{\partial V}{\partial t} = -\frac{I_{ion} + I_{stim}}{C_m} + D\nabla^2 V$$

where V is the transmembrane potential, $C_m=100$ pF is the capacitance of myocyte, I_{ion} and I_{stim} are the total transmembrane currents and stimulus current, respectively, $D=0.001$ cm²/ms is the diffusion coefficient. The diffusion term $\nabla^2 V$ was treated as the Laplace-Beltrami operator (see Supplementary information).

To study spatial dispersion of APD in bumpy geometry, we measured APD map at steady state pacing. A vertical line located at the left side of the tissue was stimulated at 2 Hz, and APD was measured across the grid at the tenth beat. APD was calculated as the time interval between the time of maximum dV/dt and repolarization to -60mV, which is related to effective refractory period. The degree of APD dispersion was estimated by standard deviation (SD) and range (max-min) of the APD. We excluded the boundary region defined by 5% of the tissue size in the analysis to eliminate the effects of tissue boundary.

We initiated spiral wave using a S1S2 cross-shock protocol. A vertical line was stimulated (S1), and further, horizontal half plane was stimulated (S2) when recovery front of S1 stimulus reached half of the tissue. After initiation of the spiral wave, we examined whether wavebreak spontaneously occurs for 5 seconds. Additionally, we re-performed all the simulations after standardizing the area of the surfaces.

In the above part, we designed the surfaces with uniformly bumpy patterns, however, real LA geometry containing both flat and complex bumpy structure has non-uniformly surface bumpiness. To examine how heterogeneous bumpiness of atrial tissue affects spiral wave dynamics, we simulated 200 random Gaussian bumpy surfaces¹⁸ and estimated wavebreak generation and AF sustainability defined as maintenance duration > 5 s. Furthermore, we also applied the bumpiness gradient and/or the ionic current gradient to determine the effects of heterogeneous bumpiness on spiral wave drift. A detailed protocol was described in Supplementary information.

2.2. Simulation of AF on 3D human LA model

We simulated an *in-silico* human LA model reflecting the LA anatomy of 14 AF patients (Table S1) who underwent radiofrequency catheter ablation (RFCA), as previously described by Hwang et al¹⁹. The study protocol adhered to the Declaration of Helsinki and was approved by the Institutional Review Board of Yonsei University Health System. The written informed consent was obtained for the use of cardiac CT and RFCA data (clinicaltrials.gov; NCT02171364). Ionic current was calculated using human atrial myocyte model¹⁷ and electrical wave conduction was modeled by the mono-domain reaction-diffusion equation on the LA geometry (CUVIA, Model: SH01, ver. 1.0, Laonmed

Inc.). We incorporated atlas-based fiber orientation to represent anisotropic electrical conduction. After the induction of AF, we calculated the density of phase singular (PS) points ²⁰ by dividing the number of PS points by the total number of nodes during 6 seconds of AF. A detailed protocol was described in Supplementary information.

2.3. Clinical electrophysiological mapping of wave dynamics parameters

We analyzed clinically obtained bipolar electrogram signals to evaluate electrical wave dynamics of AF. Electrophysiological mapping was performed during sustained AF in 30 patients with persistent AF (22 men, 62.2 ± 11.7 years old, Table S1) who underwent RFCA (see Supplementary information). The CFAE-cycle length (CL) was calculated by taking the average of time intervals between consecutive deflections. The deflections were identified as downstroke morphology between the local-maximum and the local-minimum amplitudes within a time duration of 15 ms which was set to avoid detection of far-field events. Additionally, we set a refractory period of 40 ms to avoid multiple detections of a single deflection event. CFAE was defined as CFAE-CL ≤ 120 ms.

We constructed Shannon entropy (ShEn) map as described by Ganesan et al¹⁵. Amplitude of bipolar signal was binned into voltage histogram (0.01 mV fixed bin size). The relative probability density P_i was calculated by dividing the number of counts in i th bin by the sum of counts in all bins. The ShEn was calculated as:

$$\text{ShEn} = - \sum_{i=0}^{N-1} P_i \log_2 P_i$$

where N is the total number of bins.

Additionally, we calculated approximate entropy (ApEn) map to quantify regularity of the bipolar signals²¹. We used the standard parameters with embedding dimension $m = 2$ and threshold $r = 0.1$ as described by Orozco-Duque et al¹⁶.

2.4. Calculation of curvature and surface bumpiness

We calculated the curvature of tissue geometry at each node of the surface mesh²². To represent the degree of bumpiness of the surface, we defined “surface bumpiness” by SD of the curvature as follows:

$$\text{Surface bumpiness} = \sqrt{\frac{1}{S} \iint (K - \bar{K})^2 dA}$$

where S is the surface area, K is the curvature, and \bar{K} is the average of the curvature on the surface. The surface bumpiness (SD-curvature) represents the heterogeneity of the curvature on the surface. The pulmonary veins and the mitral valve were excluded from the analysis.

2.5. Statistical analysis

All data were presented as mean \pm SD. Surface bumpiness and wave dynamics parameters were compared between the LAA and the other LA parts using a paired t-test. Linear correlation analysis was performed to determine the relationship between two continuous variables. All statistical analysis of small samples ($n<30$) were performed with nonparametric tests. The relationship between degree of APD dispersion and surface bumpiness was tested with Spearman correlation analysis. A p-value <0.05 was considered to be statistically significant.

3. Results

3.1. Spiral wave dynamics in 2D-bumpy surface

3.1.1. Dispersion of APD depending on curvature

In the 2D bumpy atrial model, we measured APD map in the steady state pacing. There was heterogeneity of APD induced by bumpy geometry in all the 24 bumpy surfaces. As shown in the flat control case (Fig. 1A), APD was significantly changed in stimulation site and exit site despite the zero-curvature of the tissue. This phenomenon is known as ‘end effect’⁹. To estimate the pure effect of curvature on APD dispersion, we excluded the boundary region in the analysis. In all the 24 bumpy surfaces, there was a linear correlation between APD and curvature (the mean of 24 Pearson coefficients was $R=0.4808\pm 0.1931$, $p<0.001$ for all 24 linear correlation tests). Additionally, APD was more heterogeneous in highly bumpy surfaces. Fig. 1D and 1E shows that the degree of APD dispersion (SD and range of APD) increased with the increase in the amplitude and the number of curves. Both SD and range of APD had positive correlation with the surface bumpiness (Spearman’s rho=0.9809 and 0.9623 respectively, both p-values <0.001).

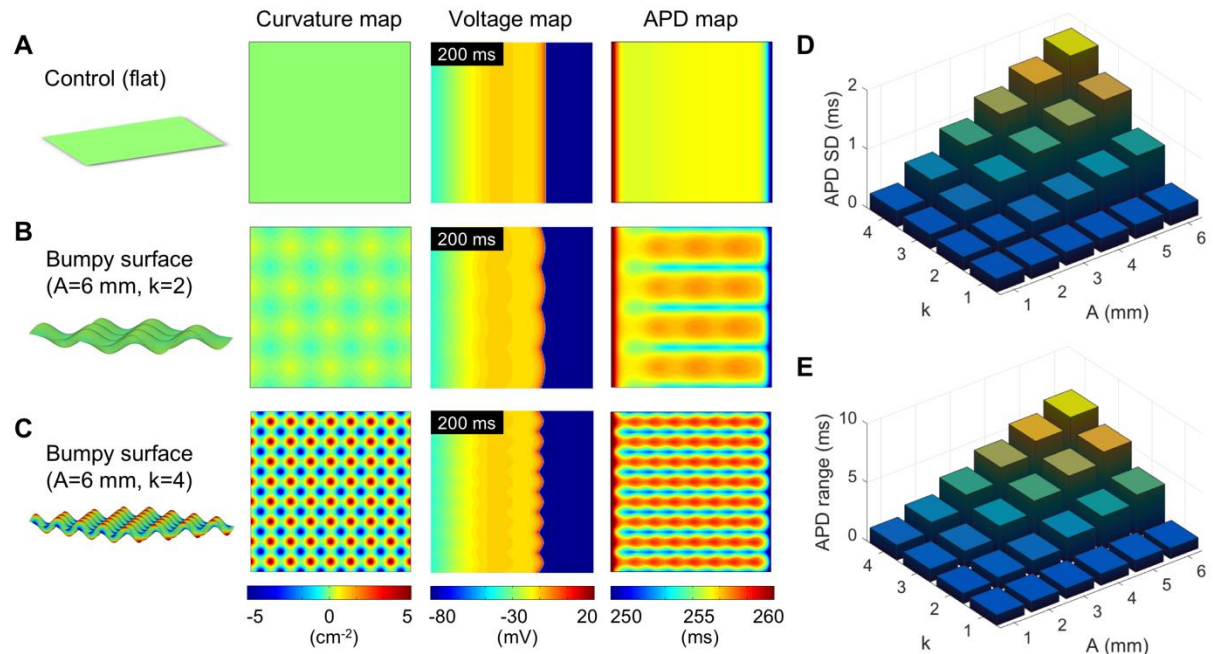


Fig. 1. Spatial dispersion of action potential duration (APD) in 2D-bumpy atrial tissue at 2 Hz

line pacing from left side. APD was spatially heterogeneous in bumpy surface and linearly correlated to curvature. (A, B, C) Curvature map, voltage map, and APD map are presented for flat control case, bumpy surface of $A=6$ mm, $k=2$, and bumpy surface of $A=6$ mm, $k=4$, respectively. A and k are the amplitude and the number of curves, respectively. (D, E) The degree of APD dispersion increased as the surface bumpiness increased.

3.1.2. Formation of wavebreak in bumpy geometry

We induced single spiral wave and examined whether wavebreak occurred spontaneously. We considered the flat tissue as a control case to compare with bumpy tissue. In the flat control case (Fig. 2A), only single spiral wave existed without any formation of wavebreak until it spontaneously terminated. The PS map with the control case shows only single trajectory of the spiral wave core. However, wavebreaks were observed in the nine surfaces of high amplitude and number of curves (Fig. 2C). As shown in Fig. 2B, wavefront was breakup into multiple wavelets when a part of the wavefront failed to propagate in the region not recovered from refractoriness. The broken ends of wavelets begin to rotate and these reentry center are shown in the PS map. In the nine surfaces with wavebreak, AF maintenance duration was prolonged compared to that of the flat control case (4.6 ± 0.6 vs. 3.7 s, $p=0.004$, Fig. S2), and surface bumpiness was higher than that in the other 15 surfaces (0.60 ± 0.53 vs. 0.09 ± 0.15 cm^{-2} , $p=0.001$, Fig. 2D). We re-performed all the simulations after standardizing the area to eliminate the effects of the tissue size on fibrillation. The results were similar to that of the original simulation (Fig. S3).

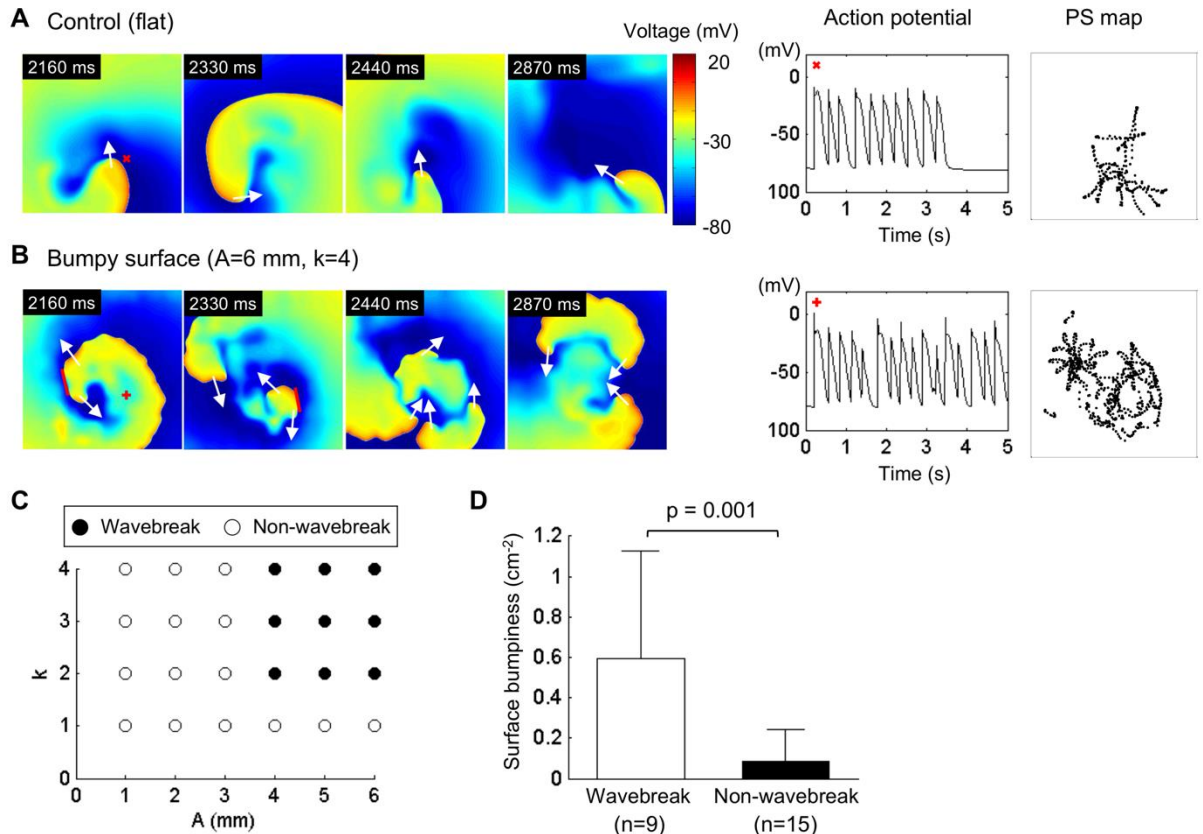


Fig. 2. Formation of spontaneous wavebreak in bumpy surface. In 2D-bumpy model, bumpy geometry could induce wavebreak without presence of electrical remodeling. (A, B) Snapshot of wave propagation, action potential, and phase singularity (PS) map are presented for flat control case and bumpy surface of $A=6$ mm, $k=4$, respectively. A and k are the amplitude and the number of curves, respectively. White arrows indicate direction of wave propagation and red lines indicate conduction block due to refractoriness. Action potential recording points are marked by red symbols. (C) Spontaneous wavebreak occurred in highly bumpy surfaces (nine black dots). Surfaces with wavebreak are marked by black dots. White dots indicate that only single spiral wave existed without any wavebreak. (D) Comparison of surface bumpiness between surfaces with wavebreak and the other cases (Mann-Whitney U test, $p=0.001$).

Furthermore, we generated 200 random non-uniformly bumpy surfaces and determined whether wavebreak spontaneously generated and whether AF maintained for 5 seconds in fibrillation state (see Fig. 3). The surfaces with wavebreak had higher surface bumpiness than that in the non-wavebreak cases ($p<0.001$), and the surface bumpiness of the AF-sustained cases was higher than that of the other cases ($p<0.001$). The logistic regression model could predict wavebreak generation ($OR=934.68$ [95% CI 105.18–8306.01], $AUC=0.9525$, $p<0.001$) and AF sustainability ($OR=45.45$ [95% CI 12.28–168.19], $AUC=0.9233$, $p<0.001$) from the surface bumpiness value.

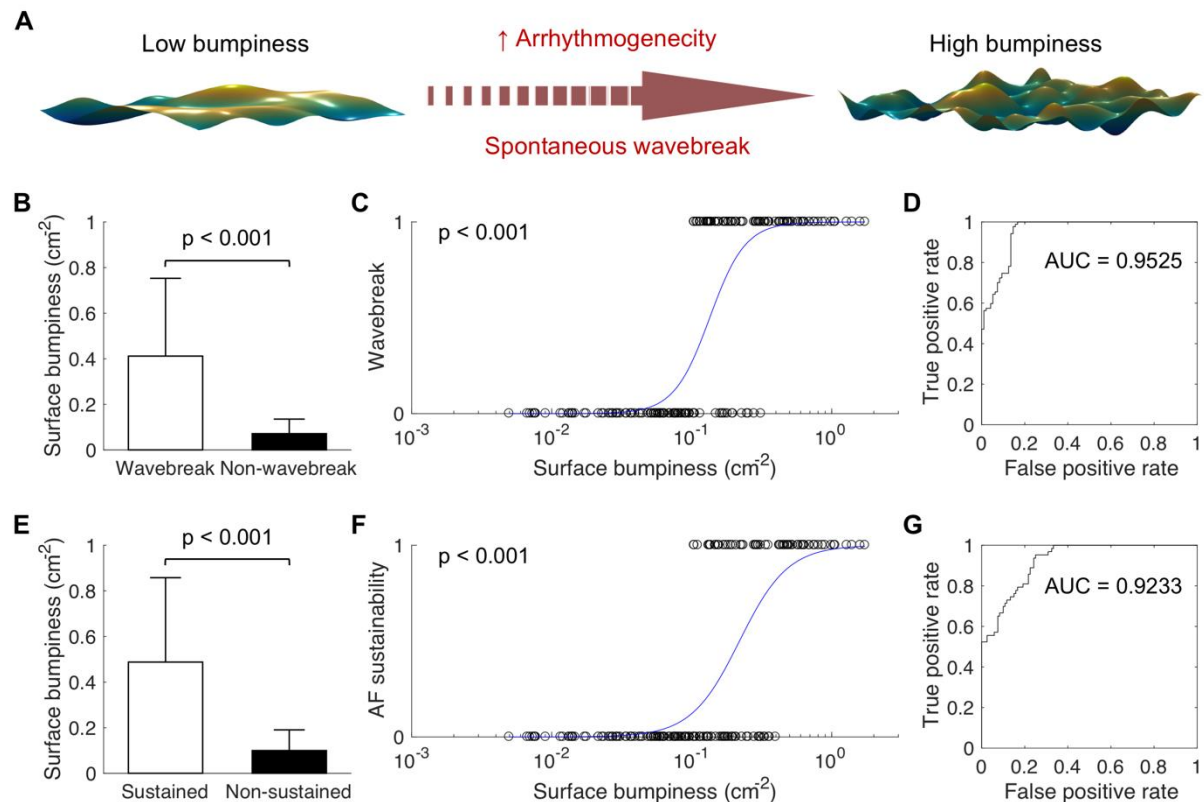


Fig. 3. Phase transition-like behavior of spiral wave dynamics. (A) Random non-uniformly bumpy

surfaces ($n=200$) were generated for testing wavebreak generation and AF sustainability (duration>5 s). (B) Comparison of bumpiness between wavebreak cases and non-wavebreak cases (t-test, $p<0.001$). (C) Logistic regression analysis between wavebreak generation and bumpiness ($p<0.001$). (D) Receiver operating characteristic analysis of the logistic regression model ($AUC=0.9525$). (E) Comparison of bumpiness between AF-sustained cases and non-sustained cases (t-test, $p<0.001$). (F) Logistic regression analysis between AF sustainability and bumpiness ($p<0.001$). (G) Receiver operating characteristic analysis of the logistic regression model ($AUC=0.9233$).

3.1.3. Drift of spiral wave against bumpiness gradient

To determine the effects of heterogeneous bumpiness on spiral wave dynamics, we simulated non-uniformly bumpy surface with bumpiness gradient. In the uniformly bumpy case (Fig. 4A), the spiral wave sustained for more than 5 s with wavebreaks, and more PS points were located at left half plane than right half plane (55.1% vs. 44.9%). However, in the surfaces with bumpiness gradient (Fig. 4B-D), more than 85% of PS points were located at right half plane, which had higher bumpiness compared with left half plane (85.7%, 96.8%, 97.4% for $\alpha=1, 2, 3$, respectively). The spiral wave drifted towards the area of higher surface bumpiness.

The combined gradient of bumpiness and ionic current showed that PS points were concentrated in the higher bumpy area and wavebreak occurred spontaneously; however, the spiral wave drift was not prominent, which might have been masked by the electrical gradient (Fig. S4).

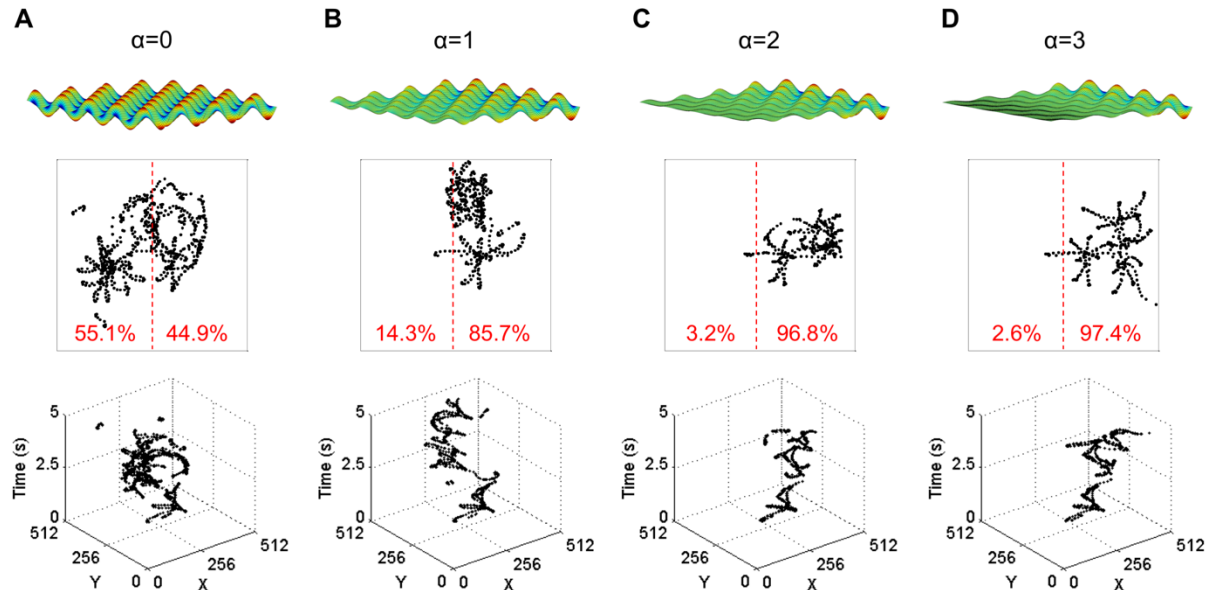


Fig. 4. Spiral wave drift and wavebreak in bumpy surface with bumpiness gradient. In 2D-bumpy model with bumpiness gradient, spiral wave drifted towards highly bumpy region (right side). Phase singularity (PS) maps (second row) and PS trajectories in space-time domain (third row) are presented for four different degrees of bumpiness gradient ($\alpha=0, 1, 2, 3$). Portion of PS points in the

right half side increased as the degree of bumpiness gradient increased (red numbers, %).

3.2. 3D human AF simulation

To determine the formation of spontaneous wavebreak in the LAA, we simulated 3D human AF model reflecting the LA anatomy of 14 AF patients. In all the cases, AF was maintained for longer than 6 seconds and wavebreak was observed in the entire LA including the LAA. Since PS is known to be closely related to wavebreak²³, we generated the PS map for 6 seconds in AF state. In both isotropic and anisotropic models, the PS density in the LAA was significantly higher than that in the other LA parts (see Fig. 5).

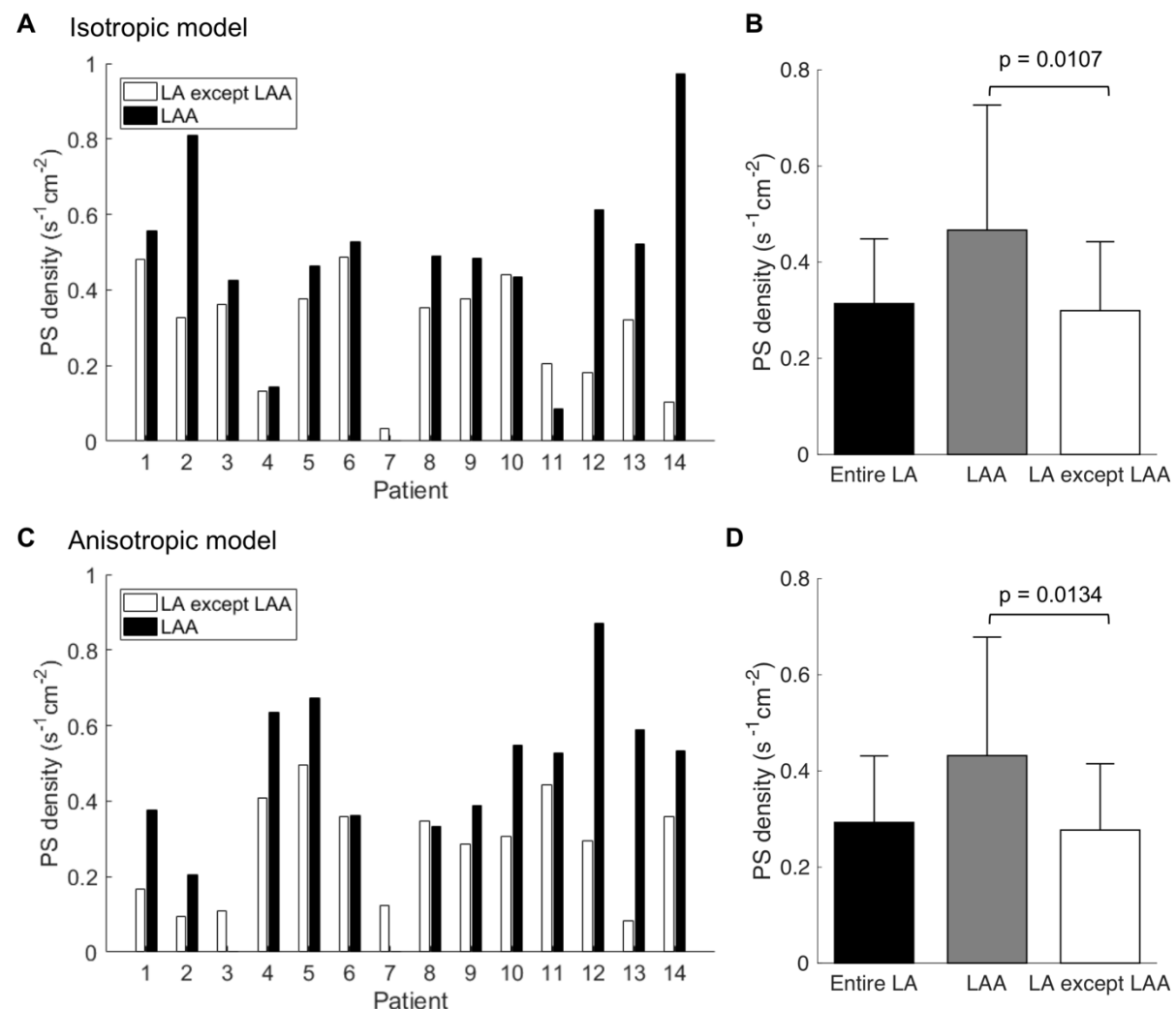


Fig. 5. Phase singularity (PS) map in 3D left atrial (LA) model (n=14). In in-silico 3D LA model of atrial fibrillation (AF), AF was successfully induced and wavebreak occurred. (A, B) Comparison of PS density between LAA and other LA parts in isotropic model (Wilcoxon signed-rank test, $p=0.0107$). (C, D) Comparison of PS density between LAA and other LA parts in anisotropic model reflecting fiber orientation (Wilcoxon signed-rank test, $p=0.0134$).

3.3. Clinical evidences for arrhythmogenic LAA

3.3.1. Curvature map of LA geometry

In 30 patients with persistent AF, we measured the curvature of LA geometry reconstructed from CT images. Fig. 6A shows that the curvature of LA geometry was heterogeneous over the entire LA. The surface bumpiness in the LAA was 5.8-fold compared with the other LA parts (1.52 ± 0.33 vs. $0.26 \pm 0.04 \text{ cm}^{-2}$, $p < 0.001$, Fig. 6E). All bumpiness values of the LAA had more than 99% probability of wavebreak generation according to the logistic regression model developed from the 2D simulation (see Fig. 3).

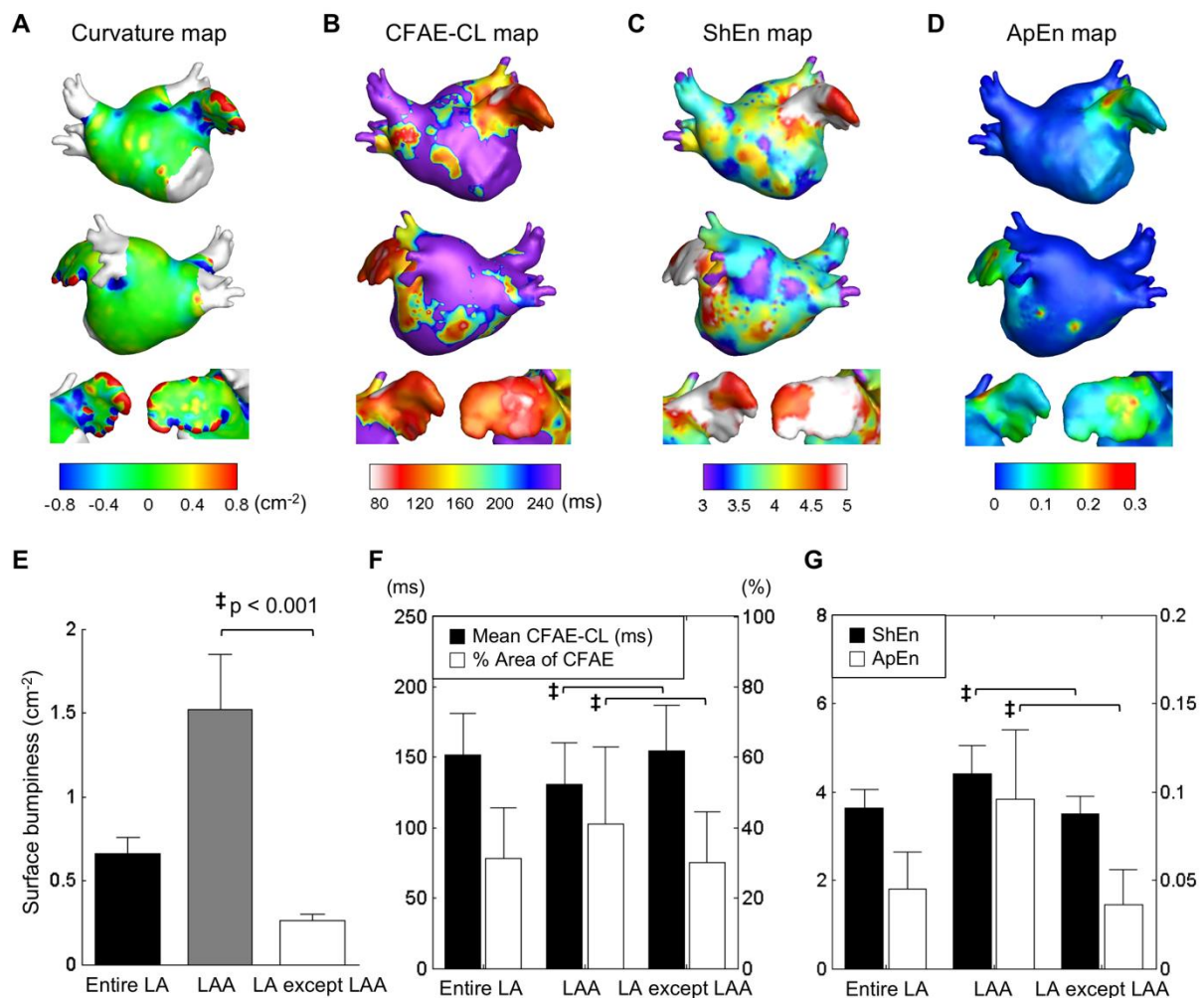


Fig. 6. The 3D left atrial (LA) mapping of curvature, complex fractionated atrial electrogram-cycle length (CFAE-CL), Shannon entropy (ShEn), and approximate entropy (ApEn) for patients with persistent AF (n=30). Wave dynamics parameters were calculated from clinically-recorded bipolar electrogram. All parameters were dominant in LA appendage (LAA). (A, B, C, D) Example of curvature, CFAE-CL, ShEn, and ApEn map, respectively. Anterior and posterior parts of LA and LAA were displayed. (E) Surface bumpiness in LAA and other LA parts (paired t-test, $p < 0.001$). (F) Mean CFAE-CL and percentage area of CFAE ($\text{CFAE-CL} \leq 120 \text{ ms}$) in LAA and other

LA parts. (G) Entropy parameters (ApEn and ShEn) in LAA and other LA parts (paired t-test, $^{\ddagger}p<0.001$).

3.3.2. Wave dynamics parameters of bipolar electrogram

We clinically obtained CFAE-CL, ShEn, and ApEn maps of the same group of 30 patients with contact bipolar electrograms taken during clinical procedures (Fig. 6B-D). Both parameters were utilized for evaluating the complexity of fractionated electrogram, which is known to be closely related to wavebreak ¹⁴. The CFAE-CL in the LAA was lower than that of the other LA parts (130.9 ± 29.4 vs. 154.7 ± 32.2 ms, $p<0.001$), and the percentage area of CFAE was higher in the LAA than that in the other LA parts (40.1 ± 22.0 vs. $30.1\pm14.5\%$, $p<0.001$, Fig. 6F). Moreover, there was an inverse relationship between the surface bumpiness of the LAA and the mean CFAE-CL of the entire LA ($R=-0.376$, $p=0.041$, Fig. S5). Additionally, both ShEn and ApEn in the LAA were higher compared to those in the other LA parts (ShEn: 4.40 ± 0.66 vs. 3.50 ± 0.39 ; ApEn: 0.10 ± 0.04 vs. 0.04 ± 0.02 ; both $p<0.001$, Fig. 6G).

4. Discussion

We discovered the arrhythmogenic role of bumpy tissue geometry using computational model of human atrial tissue. In 2D-bumpy surface model, the bumpy geometry induced APD dispersion, which led to formation of wavebreak at high surface bumpiness. Additionally, heterogeneous bumpiness caused spiral wave drift towards the region with higher bumpiness.

In 3D-LA geometry, LAA showed significantly high surface bumpiness, which produced spontaneous wavebreak in 2D-bumpy model. We performed 3D AF simulation and analyzed clinically obtained wave dynamics parameters. Both simulation and clinical data showed that the wave dynamics parameters were significantly higher in LAA compared with other LA parts.

4.1. Effects of bumpy geometry on spiral wave dynamics

The role of curvature of tissue geometry in electrical wave dynamics was primarily discovered by Davydov and Zykov¹¹. They theoretically explained the drift of spiral waves on non-uniformly curved surface. Several computational and experimental studies showed that tissue shape, structural heterogeneity, boundary features, and activation time could induce heterogeneity of refractoriness^{9,10}, which has been known to play an important role in initiation of reentry²⁴ and generation of wavebreaks^{13,25}. We discovered the quantitative relationship between APD heterogeneity and curvature of tissue geometry, and its role in wavebreak generation in bumpy surface. Additionally, we found that the bumpy tissue geometry can localize PS points by attracting the spiral wave against the bumpiness gradient. This novel finding supports that not only ionic current heterogeneity^{26,27}, but also structural heterogeneity contributes to spiral wave drift²⁸. Therefore, high surface bumpiness of tissue

geometry may be a potential source of arrhythmia.

The effect of curvature of tissue geometry can be mathematically explained by the diffusion equation of electrical conduction²⁹. Under the assumption of isotropic conduction, the diffusion term can be represented by inverse metric of the surface as $D \sum g^{ij} \partial_i \partial_j V$ where D is the diffusion coefficient and g^{ij} is the inverse metric of surface. If we define “adjusted diffusion coefficient” as $\tilde{D}_{ij} = D \cdot g^{ij}$, the diffusion term can be expressed as $\sum \tilde{D}_{ij} \partial_i \partial_j V$. Therefore, heterogeneous curvature is mathematically equivalent to heterogeneous and anisotropic conduction, which are already known to be important arrhythmogenic factors in cardiac fibrillation²⁵.

4.2. Roles of the LAA in AF maintenance

According to the study of Di Biase et al², 27% patients undergoing redo ablation showed the LAA as the trigger site of AF. Recently, they reported results of 24-month follow-up the BELIEF trial showing that the LAA isolation improved the success rate of AF treatment in the patients with long-standing persistent AF⁴. There are several potential mechanisms describing the arrhythmogenic role of the LAA⁷. Since embryological origin of the LAA is mediastinal myocardium which is related to the opening of the pulmonary vein, the LAA may similarly act as the PVs in the initiation of AF. Another anatomic consideration is the ligament of Marshall located between the LAA and the left superior PV. It contains sympathetic and parasympathetic nerves, which can form a triggering source of AF. Additionally, complex fiber orientations of the LAA may influence wave propagation and formation of localized reentry in the LAA³.

We proposed another potential mechanism for demonstrating that the bumpy morphology of the LAA may contribute arrhythmogenesis of AF. As shown in the Fig. 3, we observed critical phase transition-like phenomenon, which implies that extremely bumpy structure such as the LAA has potential to generate wavebreak and to maintain AF. The simulation result and the clinical data indicated the present of wavebreak or rotor in the LAA. According to previous studies, CFAE, ShEn, and ApEn indicates the complexity of fractionated electrogram, which is closely related to wavebreak and arrhythmogenic characteristics of AF¹⁴⁻¹⁶. Additionally, the high entropy parameters are known to be associated with rotational activation called ‘rotor’^{15,16}, which is usually produced by wavebreak at the broken ends of wavelets²³. Therefore, overall results of our study imply that the bumpy morphology of the LAA may play a pro-arrhythmic role in human AF.

4.3. Clinical implications

Although many clinical evidences have emerged to support the efficacy of the LAA isolation in controlling AF²⁻⁶, the mechanism of the LAA in the maintenance of AF is still unrevealed. We proposed a potential mechanism that the bumpy morphology of the LAA may play a pro-arrhythmic role in AF. Of course, the tissue heterogeneity and autonomic neural activity significantly contribute

to the initiation and maintenance mechanisms of arrhythmia. However, we found that anatomical bumpiness of the cardiac structures also contributes to the APD dispersion and arrhythmogenesis. Additionally, local bumpiness is linearly correlated to LA wall thickness, which is closely associated with local wave dynamics parameters³⁰. Therefore, not only the evaluation of the tissue heterogeneity but also the measurement of the surface bumpiness may contribute to the accurate mapping of potential target of arrhythmia in ablation procedure.

4.4. Limitations

In 2D simulation, we only considered periodic bumpy pattern without testing global structural heterogeneity of LAA, which must play a role in atrial arrhythmogenicity. Also, we simulated $12.8 \times 12.8 \text{ cm}^2$ tissue to avoid the issue of critical mass hypothesis³¹. However, quantitative results in 2D simulation cannot be directly compared to either simulation results of 3D-LA model or real electrical wave dynamics in patients with AF, due to the boundary effect. In our 3D AF model, we did not consider regional LA wall thickness, tissue heterogeneity, and autonomic neural activity to reduce the computational cost despite of the increasing role of intramural conduction in AF³². Also, the ionic current heterogeneity of the LAA was not considered due to the lack of detailed experimental data of full ionic current profiles on the human LAA. The sample size of 3D-patient specific modeling was relatively small, which could have affected the results. However, we confirmed reproducible results in both parametric and non-parametric analyses.

The surface bumpiness of the other LA region excluding the LAA may reflect noise, because the resolution of CT images was not sufficient to measure the accurate values of the small curvature. Also, due to technical limitations in accessing clinical APD and PS data from patients with AF, we considered CFAE-CL and ShEn as parameters for estimating electrical wave dynamics, however, CFAE-CL also reflects sequentially acquired electrograms with low spatial resolution, far-field potential, overlapped myocardial fibers, and AF drivers¹⁴. Although monophasic action potential (MAP) catheter can acquire APD data at a single point of LA, MAP catheter is not allowed for LAA mapping due to the risk of serious complication such as cardiac perforation.

We expect that global shape of the LAA may play some role in arrhythmogenicity, however, it was hard to analyze the LAA morphologies due to the limitation of patient number. Complex nonlinear relationship between structural heterogeneity and wave dynamics should be further investigated.

5. Conclusion

In the computational model of human atrial tissue, bumpy tissue morphology induced APD dispersion, which promoted formation of spontaneous wavebreak. Additionally, bumpiness gradient caused spiral wave drift in the direction of higher bumpy area. In 3D-LA geometry, surface bumpiness of the LAA is significantly higher than the other LA parts. Both simulation results and clinical data

showed that wave dynamics parameters were significantly higher in the LAA than those in the other LA parts, implying potential arrhythmogenic mechanism of the LAA in human AF.

References

- 1 Elayi, C. S. *et al.* Ablation for longstanding permanent atrial fibrillation: results from a randomized study comparing three different strategies. *Heart Rhythm* **5**, 1658-1664, doi:10.1016/j.hrthm.2008.09.016 (2008).
- 2 Di Biase, L. *et al.* Left atrial appendage: an underrecognized trigger site of atrial fibrillation. *Circulation* **122**, 109-118, doi:10.1161/CIRCULATIONAHA.109.928903 (2010).
- 3 Hocini, M. *et al.* Localized reentry within the left atrial appendage: arrhythmogenic role in patients undergoing ablation of persistent atrial fibrillation. *Heart Rhythm* **8**, 1853-1861, doi:10.1016/j.hrthm.2011.07.013 (2011).
- 4 Di Biase, L. *et al.* Left Atrial Appendage Isolation in Patients With Longstanding Persistent AF Undergoing Catheter Ablation: BELIEF Trial. *J Am Coll Cardiol* **68**, 1929-1940, doi:10.1016/j.jacc.2016.07.770 (2016).
- 5 Reissmann, B. *et al.* Durability of wide-area left atrial appendage isolation: Results from extensive catheter ablation for treatment of persistent atrial fibrillation. *Heart Rhythm* **14**, 314-319, doi:10.1016/j.hrthm.2016.11.009 (2017).
- 6 Yorgun, H. *et al.* Left atrial appendage isolation in addition to pulmonary vein isolation in persistent atrial fibrillation: one-year clinical outcome after cryoballoon-based ablation. *Europace* **19**, 758-768, doi:10.1093/europace/eux005 (2017).
- 7 Naksuk, N., Padmanabhan, D., Yogeswaran, V. & Asirvatham, S. J. Left Atrial Appendage: Embryology, Anatomy, Physiology, Arrhythmia and Therapeutic Intervention. *JACC: Clinical Electrophysiology* **2**, 403-412, doi:10.1016/j.jacep.2016.06.006 (2016).
- 8 Yamazaki, M. *et al.* Heterogeneous atrial wall thickness and stretch promote scroll waves anchoring during atrial fibrillation. *Cardiovasc Res* **94**, 48-57, doi:10.1093/cvr/cvr357 (2012).
- 9 van Oosterom, A. & Jacquemet, V. The effect of tissue geometry on the activation recovery interval of atrial myocytes. *Physica D: Nonlinear Phenomena* **238**, 962-968, doi:10.1016/j.physd.2008.08.003 (2009).
- 10 Walton, R. D., Benson, A. P., Hardy, M. E., White, E. & Bernus, O. Electrophysiological and structural determinants of electrotonic modulation of repolarization by the activation sequence. *Front Physiol* **4**, 281, doi:10.3389/fphys.2013.00281 (2013).
- 11 Davydov, V. A. & Zykov, V. S. Kinematics of spiral waves on nonuniformly curved surfaces. *Physica D: Nonlinear Phenomena* **49**, 71-74, doi:10.1016/0167-2789(91)90195-f (1991).
- 12 Kharche, S. R., Biktasheva, I. V., Seemann, G., Zhang, H. & Biktashev, V. N. A Computer

Simulation Study of Anatomy Induced Drift of Spiral Waves in the Human Atrium. *BioMed Research International* **2015**, 731386, doi:10.1155/2015/731386 (2015).

- 13 Rogers, J. M. Wave front fragmentation due to ventricular geometry in a model of the rabbit heart. *Chaos* **12**, 779-787, doi:10.1063/1.1483956 (2002).
- 14 Atienza, F. *et al.* Mechanisms of fractionated electrograms formation in the posterior left atrium during paroxysmal atrial fibrillation in humans. *J Am Coll Cardiol* **57**, 1081-1092, doi:10.1016/j.jacc.2010.09.066 (2011).
- 15 Ganesan, A. N. *et al.* Bipolar electrogram shannon entropy at sites of rotational activation: implications for ablation of atrial fibrillation. *Circ Arrhythm Electrophysiol* **6**, 48-57, doi:10.1161/CIRCEP.112.976654 (2013).
- 16 Orozco-Duque, A., Ugarte, J. P., Tobón, C., Saiz, J. & Bustamante, J. in *Computing in Cardiology 2013*. 903-906.
- 17 Courtemanche, M., Ramirez, R. J. & Nattel, S. Ionic mechanisms underlying human atrial action potential properties: insights from a mathematical model. *The American journal of physiology* **275**, H301-321 (1998).
- 18 Garcia, N. & Stoll, E. Monte Carlo calculation for electromagnetic-wave scattering from random rough surfaces. *Physical Review Letters* **52**, 1798-1801, doi:10.1103/PhysRevLett.52.1798 (1984).
- 19 Hwang, M. *et al.* Virtual ablation for atrial fibrillation in personalized in-silico three-dimensional left atrial modeling: comparison with clinical catheter ablation. *Progress in biophysics and molecular biology* **116**, 40-47, doi:10.1016/j.pbiomolbio.2014.09.006 (2014).
- 20 Lee, Y. S. *et al.* A New Efficient Method for Detecting Phase Singularity in Cardiac Fibrillation. *PLoS One* **11**, e0167567, doi:10.1371/journal.pone.0167567 (2016).
- 21 Pincus, S. M. Approximate entropy as a measure of system complexity. *Proc Natl Acad Sci U S A* **88**, 2297-2301 (1991).
- 22 Stokely, E. M. & Wu, S. Y. Surface parametrization and curvature measurement of arbitrary 3-D objects: five practical methods. *IEEE Trans Pattern Anal* **14**, 833-840, doi:10.1109/34.149594 (1992).
- 23 Chen, J. *et al.* Dynamics of wavelets and their role in atrial fibrillation in the isolated sheep heart. *Cardiovasc Res* **48**, 220-232 (2000).
- 24 Clayton, R. H. & Holden, A. V. Dispersion of cardiac action potential duration and the initiation of re-entry: a computational study. *Biomed Eng Online* **4**, 11, doi:10.1186/1475-925X-4-11 (2005).
- 25 Xie, F., Qu, Z., Garfinkel, A. & Weiss, J. N. Electrophysiological heterogeneity and stability of reentry in simulated cardiac tissue. *Am J Physiol Heart Circ Physiol* **280**, H535-545 (2001).
- 26 Calvo, C. J., Deo, M., Zlochiver, S., Millet, J. & Berenfeld, O. Attraction of rotors to the pulmonary veins in paroxysmal atrial fibrillation: a modeling study. *Biophys J* **106**, 1811-1821,

doi:10.1016/j.bj.2014.02.030 (2014).

- 27 Ten Tusscher, K. H. & Panfilov, A. V. Reentry in heterogeneous cardiac tissue described by the Luo-Rudy ventricular action potential model. *Am J Physiol Heart Circ Physiol* **284**, H542-548, doi:10.1152/ajpheart.00608.2002 (2003).
- 28 Dierckx, H., Brisard, E., Verschelde, H. & Panfilov, A. V. Drift laws for spiral waves on curved anisotropic surfaces. *Phys Rev E Stat Nonlin Soft Matter Phys* **88**, 012908, doi:10.1103/PhysRevE.88.012908 (2013).
- 29 Ogawa, N. Curvature-dependent diffusion flow on a surface with thickness. *Phys Rev E Stat Nonlin Soft Matter Phys* **81**, 061113, doi:10.1103/PhysRevE.81.061113 (2010).
- 30 Song, J. S. *et al.* Role of atrial wall thickness in wave-dynamics of atrial fibrillation. *PLoS One* **12**, e0182174, doi:10.1371/journal.pone.0182174 (2017).
- 31 Garrey, W. E. The nature of fibrillary contraction of the heart—Its relation to tissue mass and form. *The American journal of physiology* **33**, 397-414, doi:10.1152/ajplegacy.1914.33.3.397 (1914).
- 32 Hansen, B. J. *et al.* Atrial fibrillation driven by micro-anatomic intramural re-entry revealed by simultaneous sub-epicardial and sub-endocardial optical mapping in explanted human hearts. *Eur Heart J* **36**, 2390-2401, doi:10.1093/eurheartj/ehv233 (2015).